The ultraviolet Martian dayglow observed with NOMAD/UVIS on ExoMars Trace Gas Orbiter

Lauriane Soret[1], Jean-Claude Gérard[1], Benoît Hubert[1],
A.C. Vandaele[2], I. R. Thomas[2], B. Ristic[2], Y. Willame[2],
Nicholas Schneider[3], Sonal Jain[3], Sumedha Gupta[3],
J. P. Mason[4], M. R. Patel[4]

[1] LPAP, STAR Institute, Université de Liège, Belgium
[2] Royal Belgian Institute for Space Aeronomy, Brussels, Belgium
[3] Laboratory for Atmospheric and Space Physics, Boulder, CO, United States
[4] School of Physical Sciences, The Open University, Milton Keynes, UK

Abstract

The Trace Gas Orbiter (TGO) has been orbiting Mars since 2016 with the Nadir and Occultation for MArs Discovery (NOMAD) UltraViolet and Visible Spectrometer (UVIS) instrument on board. Focusing on limb observations recorded in the ultraviolet (UV) part of the NOMAD/UVIS spectra, we describe here the CO Cameron bands, CO_2^+ ultraviolet doublet and Fox-Duffendach-Barker (FDB) bands and [OI] UV emissions. Averaged limb profiles are presented, showing that the strongest brightness and the highest peak altitudes are reached near perihelion. Ratios between the UV emissions are also estimated and compared with previous observations from Mariner and Mars Express. NOMAD/UVIS is the first instrument able to simultaneously acquire data both in the UV and the visible in the Mars atmosphere so that the oxygen green line at 557.7 nm and its UV counterpart at 297.2 nm, both originating from the same $O(^1S)$ upper state level, may be directly compared. A mean ratio of 15.8 is derived, in close agreement with *ab initio* calculations. The spectral composition of the CO_2^+ FDB system that have not been observed entirely since the Mariner missions in the 1970s is analyzed. According to the spectral composition of the FDB bands, we show that this emission is produced at ~70 % by photoionization of CO_2 (which populates the shorter wavelengths of the spectrum) and ~30 % by resonance scattering of solar radiation (which populates longer wavelengths). No evidence of a change with altitude in the CO_2^+ FDB spectral composition is observed in the NOMAD/UVIS spectra.

Plain language summary

Dayglow is an atmospheric emission occurring on the illuminated side of a planet. This phenomenon occurs when atmospheric atoms or molecules interact with incoming solar radiation that produce excited atoms and molecules. When these atoms and molecules de-excite radiatively, they release photons at specific wavelengths and altitudes, generating airglow. Several space missions since the 1970s observed the Mars ultraviolet dayglow. The NOMAD/UVIS instrument, currently orbiting Mars since 2016, is providing new insights on this phenomenon. In this study, we describe the results of the observations of the Martian UV dayglow by NOMAD/UVIS. We show that the strongest emissions occur at higher altitudes, when the planet is closest to the Sun. We also estimate the intensity ratios between the emissions and compare our results with previous observations from Mariner and Mars Express. The CO_2^+ emission between 300 and 400 nm is also detected for the first time since the Mariner missions in the 1970s. The production mechanisms can be deduced by analyzing the spectral distribution of this emission. We conclude that photoionization

of CO_2 represents ~70% of its production while resonance scattering of solar radiation accounts for ~30 %. This conclusion was predicted by models but this is the first time that observations validate these simulations. This statement is true at all the observed altitudes.

Key points

- The Mars UV dayglow emissions from CO Cameron, CO_2^+ UVD and [OI] UV and CO_2^+ FDB are analyzed using NOMAD/UVIS limb spectra.
- The controversial 557.7nm/297.2nm intensity ratio derived from those simultaneous measurements is highly reliably determined.
- The full wavelength range of the CO_2^+ Fox-Duffendach-Barker band system is detected for the first time since Mariner.

Keywords

Mars, atmosphere, dayglow, ultraviolet, airglow

1. Introduction

Dayglow is a form of non-thermal atmospheric emission occurring on the illuminated side of a planet. This phenomenon is produced when atmospheric atoms or molecules interact with incoming solar radiation. Direct resonant absorption and scattering of the solar light make a first contribution to the dayglow. Ionization of the atmospheric gas by energetic solar radiation, mainly extreme ultraviolet and X-ray photons, produces photoelectrons carrying an excess energy. When these electrons collide with atmospheric atoms and molecules, they can transfer energy to these targets and trigger a broad set of photochemical reactions, many of which produce excited atoms and molecules. When these atoms and molecules de-excite radiatively, they release photons at specific wavelengths and altitudes, generating airglow. Several space missions since the 1970s observed the Mars ultraviolet dayglow. The NOMAD/UVIS instrument, currently orbiting Mars since 2016, is however providing new insights on this phenomenon. In this study, we describe the results of the observations of the Martian UV dayglow by NOMAD/UVIS.

1.1. Martian ultraviolet dayglow emissions

Martian ultraviolet dayglow spectra were first observed during the Mariner 6 and 7 flybys, with a spectral resolution of 1 nm between 110 and 210 nm and 2 nm between 190 and 430 nm (Barth et al., 1971). Their analysis revealed the presence of the CO ($a^3\Pi$-$X^1\Sigma$) Cameron and ($A^1\Pi$-$X^1\Sigma^+$) Fourth Positive bands, the CO_2^+ ($A^2\Pi_u$-$X^2\Pi_g$) Fox-Duffendach-Barker (FDB) bands and ($B^2\Sigma_u^+$-$X^2\Pi_g$) ultraviolet doublet (UVD) at 288-289 nm, the HI Lyman-α line at 121.6 nm, the OI UV multiplets at 130.4, 135.6 nm and 297.2 nm and the CI emissions at 156.1 and 165.7 nm. They analyzed the altitude distribution and excitation mechanisms of these emissions and drew conclusions concerning the atomic oxygen and CO_2^+ abundance. They found that the altitude distribution of all the emissions was the same, except for the Lyman-α and OI 130.4 nm lines and part of the CO_2^+ FDB bands. They also derived temperatures of the upper atmosphere from the scale height of several emissions.

Stewart (1972) conducted a detailed study of the limb profiles of the CO Cameron, the CO_2^+ UVD and the FDB bands collected during Mariner 6 and 7 limb scans. However, the UVD and FDB bands were saturated below 140 km, so that the peak intensity and altitude of these emissions could not be determined. He also concluded that the spectral features in the middle ultraviolet (MUV) arise predominantly from the interaction of solar photons with CO_2, the major atmospheric constituent, unlike the far ultraviolet emissions that originate

from minor constituents. The [OI] 297.2 nm line (Barth et al., 1971; Stewart, 1972) limb intensity reached 20 kR (kilorayleigh) at 120 km but no usable measurements were available at lower altitude. Fox and Dalgarno (1979) and Jain and Bhardwaj (2012) implemented models indicating that solar fluorescence is a negligible source of the CO_2^+ UVD emission, but may be important for the FDB bands.

The ultraviolet spectrometer on board Mariner 9 obtained spectra in the 190-340 nm range every 3 seconds during 120 days (Barth et al., 1972; Stewart et al., 1972). They confirmed that most emissions, with the exception of Lyman-α and OI emissions are excited by the interaction of solar ultraviolet radiation with CO_2.

The Mars far ultraviolet (FUV) disk spectrum was measured between 82 and 184 nm at a resolution of 0.4 nm with the Hopkins Ultraviolet Telescope (HUT) on board the Space Shuttle (Feldman et al., 2000). Beyond 125 nm, it is dominated by the CO Fourth Positive ($A^1\Pi$-$X^1\Sigma^+$) band system and strong OI and CI multiplets. The distribution of the CO Cameron and CO_2^+ UVD bands have then been measured in the dayglow with the SPectroscopy for the Investigation of the Characteristics of the Atmosphere of Mars (SPICAM) instrument on board Mars Express (MEx). The results were described and analyzed by Bertaux et al. (2006), Leblanc et al. (2006), Shematovich et al. (2008), Simon et al. (2009), Cox et al. (2010), Stiepen et al. (2015) and González-Galindo et al. (2018). They found that the peak brightness and altitudes of CO_2^+ UVD and CO Cameron are, on average, 23 kR at 119 km and 120 kR at 124 km, respectively. However, Montmessin et al. (2017) explained that, because of an increase of the effective area, the calibration had to be corrected. Hereafter, previous intensities derived from SPICAM data are corrected to account for this updated detector effective area.

The oxygen 297.2 nm line, originating from the O(^{1}S) level, was observed in the SPICAM dayglow spectra analyzed by Leblanc et al. (2006). It was weaker relative to CO Cameron and CO_2^+ UVD in the SPICAM data than in the Mariner 9 data. Fox and Dalgarno (1979) listed photodissociative excitation by solar EUV radiation and photoelectron impact dissociative excitation of CO_2, photoelectron impact on O(^{3}P) atoms and dissociative recombination of O_2^+ as potential sources of O(^{1}S) atoms. Their model calculations indicated that photodissociation of CO_2 was by far the dominant source, especially for the lower peak region. The same list of processes was used by Gérard et al. (2020, 2021) to successfully compare their model simulations with the characteristics of the OI 557.7 nm emission that originates from the same O(^{1}S) level as the 297.2 nm airglow.

Even though the spectral range of the SPICAM instrument on board MEx extends up to 320 nm, its sensitivity rapidly decreased beyond ~300 nm. No useful information about the CO_2^+ FDB bands could thus be collected.

An extensive set of ultraviolet dayglow spectra has been collected with the Imaging UltraViolet Spectrograph (IUVS) on board the Mars Atmosphere and Volatile Evolution Mission (MAVEN) orbiter since November 2014 (McClintock et al., 2015; Jain et al., 2015). The spectral coverage of the MUV channel extends up to 330 nm. Many different spectral features have been analyzed and modeled. Gérard et al. (2019) presented averaged limb profiles of the Cameron bands and UV doublet. They compared them with numerical simulations using neutral densities from the Mars Climate Database (MCD, Millour et al., 2012) adapted to the conditions of the observations. They showed that the altitude and simulated peak intensities of the UVD and Cameron bands are in good agreement with the observations. The limb intensity distribution of the [OI] 297.2 nm emission has been described by Gkouvelis et al. (2018). They found that this emission presents a double maximum and that the altitude of its lower peak varies during the course of a Martian year as a result of the seasonal expansion of the atmosphere as the planet approaches perihelion. Gkouvelis et al. (2020) showed that the altitude of the lower intensity peak follows the location of the 0.39-mbar level and depends on the atmospheric dust load of the lower atmosphere. Jain et al. (2015) reported that only the CO_2^+ FDB (3-0) and (2-0) bands could be analyzed in the MAVEN/IUVS spectra. Based on 744 altitude profiles, they estimated the peak altitude to be located at ~130 km.

Recently the Nadir and Occultation for MArs Discovery (NOMAD) UltraViolet and Visible Spectrometer (UVIS) instrument on board the Trace Gas Orbiter (TGO) has been orbiting Mars since October 2016. So far, only the visible part of the dayglow spectra was described. The oxygen green line at 557.7 nm was detected for the first time in the Mars atmosphere (Gérard et al., 2020). Statistical studies of this emission were performed by Gérard et al. (2021), Aoki et al. (2022) and Soret et al. (2022). The intensity ratio I(557.7 nm/I(297.2 nm) could have been estimated for the first time in the Mars atmosphere. A value of 16.5 ± 0.4. was determined from a limited sample of NOMAD/UVIS dayglow observation (Gérard et al., 2020). This value agreed with the NIST recommended value of 16.7 (Kramida, 2022).

In this study, we concentrate on the ultraviolet part of the UVIS dayglow spectra. The UVIS instrument is described in Section 1.2. A validation of our data processing and calibration is performed with a comparison to the MAVEN/IUVS data in Section 2. Section 3 presents an averaged NOMAD/UVIS dayglow spectrum and Section 4 focuses on the intensity ratio between the OI 557.7 nm and 297.2 nm emissions that both originate from the O(^{1}S) metastable state. In Section 5, we generate limb profiles of the dayglow emissions, study their seasonal variations and calculate UV emission ratios. Finally, in Section 6, we compare the observed emissions with model simulations and discuss the relative importance of their different source processes.

1.2. The ExoMars/TGO/NOMAD/UVIS instrument

TGO started orbiting Mars on 19 October 2016 on a quasi-circular orbit at about 400 km, inclined by 74° relative to the equator. On board, the NOMAD/UVIS spectrometer was mainly designed to perform solar occultations in the ultraviolet and measure ozone absorption in backscattered solar radiation. Detailed information about the UVIS spectrometer can be found in Patel et al. (2017) and Vandaele et al. (2018a, 2018b). In a special mode, limb measurements are also performed between 200 and 650 nm, with a spectral resolution that varies from 1.2 nm at 200 nm to 1.6 nm at 650 nm. Part of the CO Cameron bands, the CO_2^+ UV doublet, the FDB bands and the [OI] line at 297.2 nm can consequently be observed simultaneously with the oxygen forbidden transitions at 557.7 and 630-636.4 nm (Gérard et al., 2020, 2021; Soret et al., 2022).

In this study, only limb pointing observations are used. They can be made either in the inertial mode (where a whole range of altitudes of the tangent point is scanned) or the tracking mode (the altitude of the tangent point is constrained to remain almost constant during the time of the observation while a latitudinal scan is performed). In the limb tracking mode, the tangent altitude usually stabilizes within ~20 km during the course of an observation sequence. Acquisition of inertial limb observations began on 23 April 2019 (MY 35, Ls = 15°) while limb tracking observations started on 3 February 2021 (MY 35, Ls = 358°). Regarding the data processing pipeline, the instrumental background and dark current (DC) on the CCD frame is first removed. In a second step, the noise is corrected from cosmic rays, anomalous and hot pixels. The 81 fully illuminated CCD lines are binned to increase the

signal-to-noise ratio of the spectrum. Finally, the count rate is converted into brightness units (kR) based on laboratory measurements obtained during the ground-based and in-flight calibration campaigns. During these dayglow limb measurements, stray light can easily be removed thanks to the non-illuminated regions at the top and bottom parts of the CCD. However, the background noise removal is important as the dayglow signal is very faint. In addition to the statistical error on the brightness, a possible systematic error is associated with the uncertainties of the relative instrumental calibration estimated to be less than 10%. More details about calibration can be found in Willame et al. (2022).

2. NOMAD/UVIS and MAVEN/IUVS concurrent observations

The most recently published UV dayglow observations have been performed by IUVS (McClintock et al., 2015; Jain et al., 2015) onboard the ongoing NASA MAVEN mission. It has been orbiting Mars since 21 September 2014 along an elliptical orbit and has acquired a considerable amount of data. The aim of the MAVEN/IUVS instrument is to study the Martian upper atmosphere in the far (110–190 nm) and the middle (180–340 nm) ultraviolet. In the following paragraphs, we compare NOMAD/UVIS limb measurements with quasi-concurrent MAVEN/IUVS limb observations (Deighan, 2018). Coincidental observation of the same region by both spacecraft only occur seldom. We searched through the NOMAD/UVIS database looking for MAVEN/IUVS limb observations acquired at the same date, at a similar solar zenith angle (SZA) and latitude. The best match was found on 8 July 2020. The UVIS observation started at 11:40:46 UTC time and two IUVS scans performed this day during MAVEN orbit #11894 were made at about the same time in the vicinity of the NOMAD observations (about the same latitudes and SZA). Figure 1a shows the comparison between the averaged 110-130 km UVIS (black) spectra and the two corresponding IUVS (red) spectra (scans #5 and #6). IUVS Level 1 C (L1C; Schneider et al., 2020; 2021; Jain et al., 2015) spectra are corrected for detector dark current, background subtracted and calibrated in physical units. The MUV brightness data carry an estimated systematic uncertainty of 30%. Cleaned data are archived in the NASA Planetary Data System (PDS, see Data Availability Statement). Despite the fact that observations are not perfectly simultaneous in time and location, the agreement between the NOMAD and MAVEN spectra is excellent. The linear Pearson-R correlation coefficient of the spectra reaches 0.85. We thus confirm that

MAVEN/IUVS and NOMAD/UVIS dayside limb observations provide similar ultraviolet brightness under similar observing conditions. Other quasi-simultaneous observations with the two instruments confirmed the agreement.

Limb profiles of selected UV dayglow emissions can be compared as well. The procedure to generate average limb profiles based on individual spectra will be described in Section 5.1 but it is important to underline here that NOMAD/UVIS spectra observations only cover the passband longward of 200 nm, thus missing the short wavelengths bands of the CO Cameron system below 200 nm. Based on the comparison with the complete MAVEN/IUVS CO Cameron spectrum, the UVIS missing part of the Cameron bands corresponds to 22 % of the total Cameron emission. Hereafter, intensities retrieved from the UVIS spectra between 200 and 260 nm are multiplied by 1.22 to compensate for the missing bands. The limb brightness of the CO Cameron, CO_2^+ UVD and [OI] UV emissions is plotted as a function of altitude of the tangent point in panels 1b, Figure 1c and 1d, respectively. Here again, we compare NOMAD/UVIS (black circles) and MAVEN/IUVS (red lines) measurements. The agreement between the two instruments is quite good, especially for the UV doublet and [OI] 297 nm emissions. The brightness at the peak differs by 6 to 17 %, depending on the emission. The peak altitudes of the emissions are in excellent agreement: a difference of 5, 2 and 10 km is observed for the CO Cameron, [OI] and UVD emissions, respectively. We definitely establish that MAVEN/IUVS and NOMAD/UVIS provide similar results that can directly be compared.

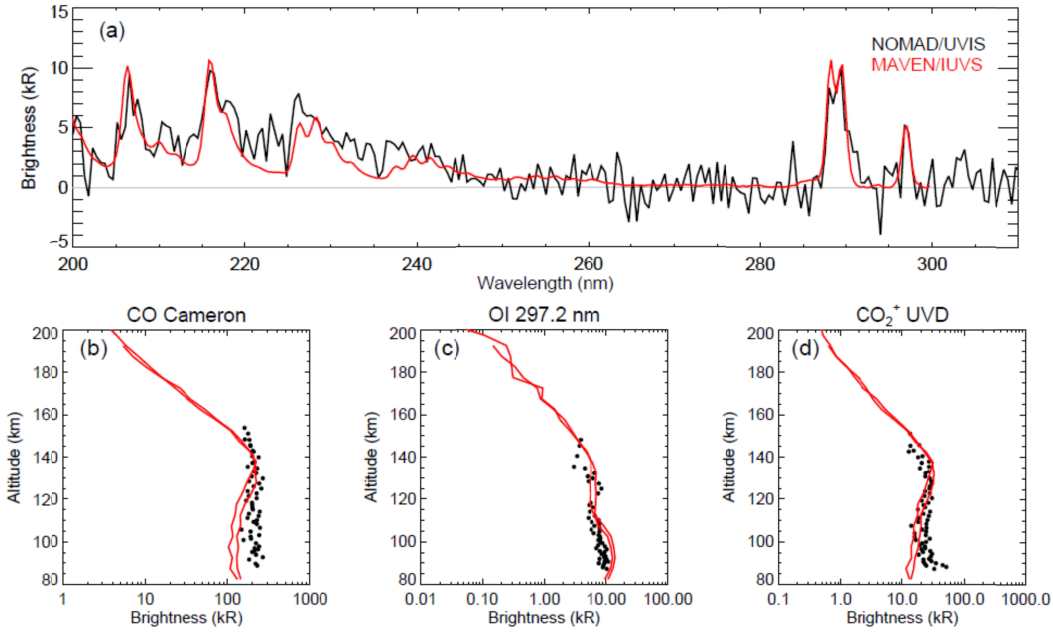

Figure 1: a) An averaged NOMAD/UVIS spectrum (black) is shown together with the average of two nearly coincident MAVEN/IUVS spectra (red, orbit #11894, UTC times 11:38:59 and 11:40:49), acquired on the 2022/07/08 between 110 and 130 km. MAVEN/IUVS (red) limb profiles of the CO Cameron (b), OI at 297.2 nm (c) and CO_2^+ UVD (d) are overplotted on top of NOMAD/UVIS (black) measurements.

3. Average UV dayglow spectrum

The NOMAD/UVIS limb database used in this study is composed of a total of 214 orbits, acquired between 23 April 2019 (MY 35, Ls = 15°) and 31 October 2022 (MY 36, Ls = 330°), thus covering almost two Martian years. Among these, 145 limb observations have been performed on the dayside of the planet. The geometry of all the spectra acquired for a SZA less than 70° and a tangent point altitude between 50 and 200 km is illustrated in Figure 2. It shows the altitude and latitude of the 7164 dayside limb spectra. Figure 2b indicates that all altitudes are well covered by these observations (at least 100 observations per altitude bin) and is thus a representative sample for a statistical study. Panels 2c and 2d respectively represent the latitudinal and solar longitudinal distributions of the observations. Owing to the small orbital inclination, low latitudes have been more frequently observed than other regions. Seasons are also well covered with the exception of the northern summer period.

Figure 3 shows the average spectrum generated using all UVIS spectra between 105 and 135 km to focus on the altitudes of the maximum of the UV emissions and to limit contamination either by solar scattered light at low altitude or sky background at higher ones. Spectra have been corrected by subtracting the average background noise levels that were estimated in the [249:253], [279:287], [292.5:294.5], [300:304] and [371:375] -nm wavelength intervals and connected together either with polynomial (for the CO Cameron and CO_2^+ FDB systems) or linear (for the other line emissions) fits. Several of the CO Cameron bands between 200 and 270 nm can be seen in this averaged spectrum, as well as the CO_2^+ UVD (288-289 nm) and the [OI] emission at 297.2 nm. The A $^2\Pi_u$-X $^2\Pi_g$ FDB bands were first identified in a celestial object by Swings and Page (1950) in the spectrum of comet Bester. A detailed study of the excitation mechanisms of both the FDB bands and the UV doublet in cometary spectra was published by Festou et al. (1982). For the first time since the detection in the Mars atmosphere by the Mariner missions in the 1970s (Barth et al., 1971), a large fraction of the CO_2^+ FDB system between 300 and 400 nm is observed with NOMAD/UVIS. The FDB Mariner spectrum is shown in red in Figure 3. This spectrum has been generated using four observations acquired between 160 and 180 km. Intensities have been multiplied by 2 to match the NOMAD/UVIS spectrum (in black). This scaling factor has been applied because observing conditions were not the same: different solar activity, SZA, latitude and longitudes. The entire FDB system has not been observed since Mariner in the Mars atmosphere. Indeed, MAVEN/IUVS detects the (3,0) and (2,0) bands (Jain et al., 2015) but only NOMAD/UVIS is currently able to observe all the bands. As for the comparison shown with MAVEN/IUVS in Section 2, the agreement between the Mariner and NOMAD spectra is excellent. Hereafter, a fit (using a least mean-squares method) of the Mariner FDB spectrum is performed on each UVIS spectrum between 302 and 399 nm to retrieve the brightness of the full CO_2^+ FDB band system in the NOMAD/UVIS spectra.

No other emission has been identified above the background noise level in the NOMAD/UVIS spectra.

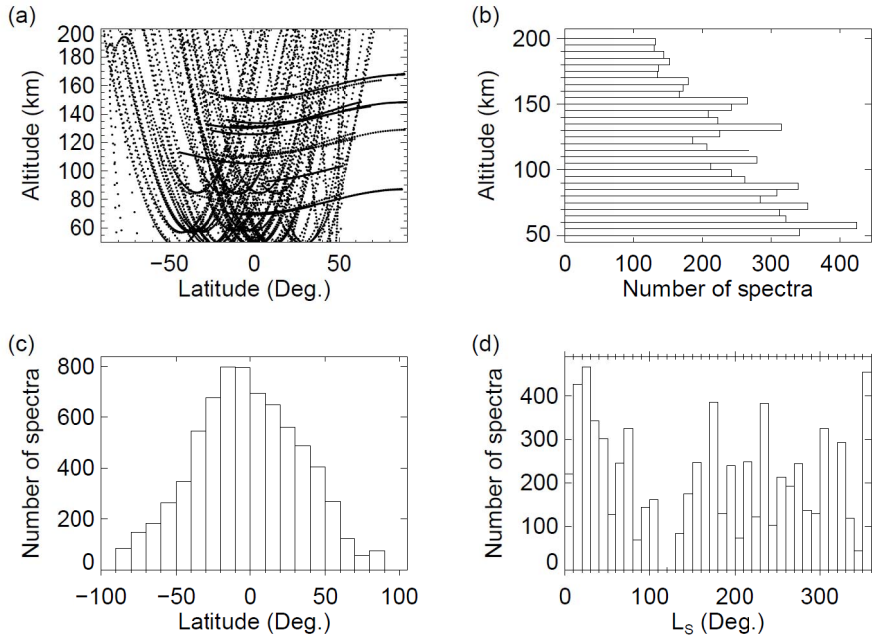

Figure 2: Geometry of the dayside limb observations used for this study, for a SZA less than 70°. (a) Parabolas represent inertial limb observations while nearly horizontal lines correspond to limb tracking data at different altitudes. Distributions of the spectral observations according to: (b) altitude, (c) latitude and (d) solar longitude.

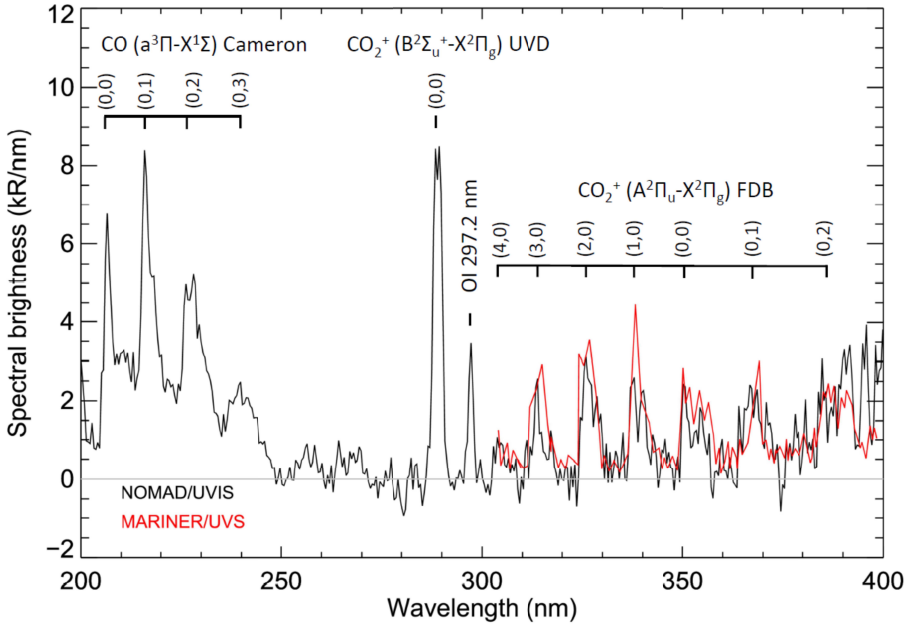

Figure 3: Average of 1480 spectra acquired on the dayside between 105 and 135 km. Four distinct emissions can be observed: several of the CO Cameron bands between 200 and 270 nm, the CO_2^+ UVD (288-289 nm), the [OI] emission at 297.2 nm, as well as a large fraction of the CO_2^+ FDB

system starting from 300 nm. The Mariner/UVS CO_2^+ FDB spectrum from Barth et al. (1971) scaled to the IUVS spectrum is overplotted in red.

4. The oxygen visible/UV ratio

The forbidden oxygen lines at 557.7 and 297.2 nm both originate from the same O(^{1}S) excited level. Therefore, their relative intensity corresponds to the ratio of the two transition probabilities of the $^1S \rightarrow {}^1D$ and $^1S \rightarrow {}^3P$ transitions, which is constant at low pressure levels and equal to 16.7, according to the National Institute of Standards and Technology (NIST) (Kramida, 2022). The value of this ratio has been controversial for many years as the theoretical value differed from that observed in the terrestrial airglow by nearly a value of 2: ratios of 9.8 ± 1.0 and 9.3 ± 0.5 were found in the terrestrial nightglow and in the Earth aurora, respectively (Slanger et al., 2006; Gattinger et al., 2009). However, as explained by Gérard et al. (2020), these values rely on the instrumental calibration of two distinct spectral windows. Yet, this value is of great importance since this ratio is used to calibrate the ultraviolet and visible spectral regions. Recently, Gérard et al. (2020) measured this ratio in the Martian dayglow based on 16 inertial limb scans by NOMAD/UVIS. Contrary to previous studies based on visible and UV intensities measured with different instruments and with different absolute calibration, the NOMAD/UVIS instrument allows to directly compare the relative ratio of the two emissions. The uncertainty of the relative spectral calibration between the visible and the ultraviolet domains is estimated less than 10%. Based on 104 spectra with a high signal to noise ratio, Gérard et al. (2020) found a value of 16.5 with a standard error on the weighted means of 0.4, in close agreement with the theoretical value of 16.7. Using the NOMAD/UVIS dayside limb observations, Soret et al. (2022) found that the main emission peak of the oxygen green line was statistically located at 82.5 km with a brightness of 115 kR but did not perform the same analysis for the UV part of the UVIS spectra. However, with its extended spectral coverage from 200 to 650 nm, UVIS is now able to measure simultaneously both the oxygen UV and visible emissions in the Martian dayglow. In this study, we use this opportunity to re-examine the value of this ratio, taking advantage of the larger number of limb observations at the altitude of the emission peak now available.

Figure 4 shows the 557.7nm/297.2nm intensity ratio averaged in 5-km altitude bins. The variations with altitude have no physical basis and are probably due to the varying signal to noise ratio and imperfect background removal of the solar scattered radiation. The mean value is 15.8, with an absolute uncertainty due to the background noise level in the vicinity of the emissions of 2.4. This ratio is in close agreement with the value recommended by NIST (vertical grey line) and the earlier determination by Gérard et al. (2020).

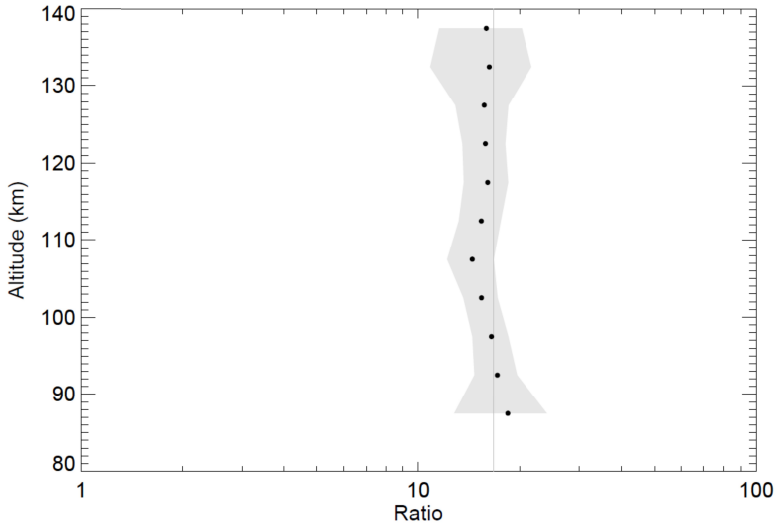

Figure 4: Measurements of the intensity ratio of the 557.7 nm/297.2 nm oxygen dayglow emissions (black dots). The limb data have been binned into 5-km intervals. The vertical line indicates the theoretical value of 16.7. The grey color represents an estimate of the value of the absolute uncertainty of the ratio, based on the 1-σ deviation of the background noise in the neighborhood of the emissions.

5. Limb profiles

5.1. Average limb profiles

As was shown in Figure 2a, 7164 spectra have been collected in both the inertial and tracking limb modes by UVIS on the dayside and are well distributed in altitude. In order to generate average limb profiles in the UV (as previously done for the visible by Soret et al., 2022), all spectra have been grouped into 5 km bins (30 bins from 50 to 200 km) of altitude

of the tangent point of the observation. Then, an average spectrum is estimated in each bin and corrected from the background noise (see Section 3). Finally, the brightness of every UV feature is extracted. For each dayglow emission, an averaged brightness is thus obtained at each altitude, which allows the construction of a mean limb profile. Such limb profiles are plotted with black dots in panels (a) to (d) of Figure 5 for the CO Cameron, the OI 297.2, the CO_2^+ UVD and FDB emissions, respectively. The grey color represents an estimate of the value of the 1-σ deviation of the noise in the neighborhood of the emissions.

The Cameron, UVD and FDB emissions all peak at 122.5 km. The OI 297.2-nm emission, similarly to the oxygen green line (Gérard et al, 2020; Aoki et al., 2022; Soret et al., 2022), presents two peaks, the main one being located at 92.5 km. Additionally, colored dots represent values of measurements from previous observations: red dots refer to Mariner 6 and 7 (Barth et al., 1971; Stewart, 1972) for the UVD and FDB emissions and Mariner 9 (Stewart et al., 1972) for the CO Cameron bands, green dots to MAVEN/IUVS (Gkouvelis et al., 2018; Gérard et al., 2019) and blue dots to MEx-SPICAM missions (Cox et al., 2010). Regardless of the emission, NOMAD/UVIS brightness values are always larger than MEx/SPICAM measurements and smaller than MAVEN/IUVS and Mariner/UVS observations. The altitudes of the peaks are in very good agreement with previous missions except for Mariner that detected emission peaks higher in the atmosphere. However, we point out once again that NOMAD/UVIS results presented here correspond to average values, mixing all seasons, longitudes and latitudes for solar zenith angles up to 70°, while measurements from previous missions were made under specific conditions. This is for example the case of the MAVEN/IUVS data: while IUVS performs observations under various conditions, the observations presented here correspond to values that have been measured between October 2014 and June 2018. This time period actually corresponds to the beginning of the decreasing phase of solar cycle 24 (i.e. a somewhat high solar activity). This is in contrast with the UVIS limb observations that started in April 2019, a period of deep solar minimum. Mariner measurements were limited to a few observations, acquired during a very high solar activity period (solar cycle 20) near perihelion (when the Mars atmosphere is expanding) of MY 9. MEx/SPICAM observations, on the other hand, have also been performed during a solar minimum.

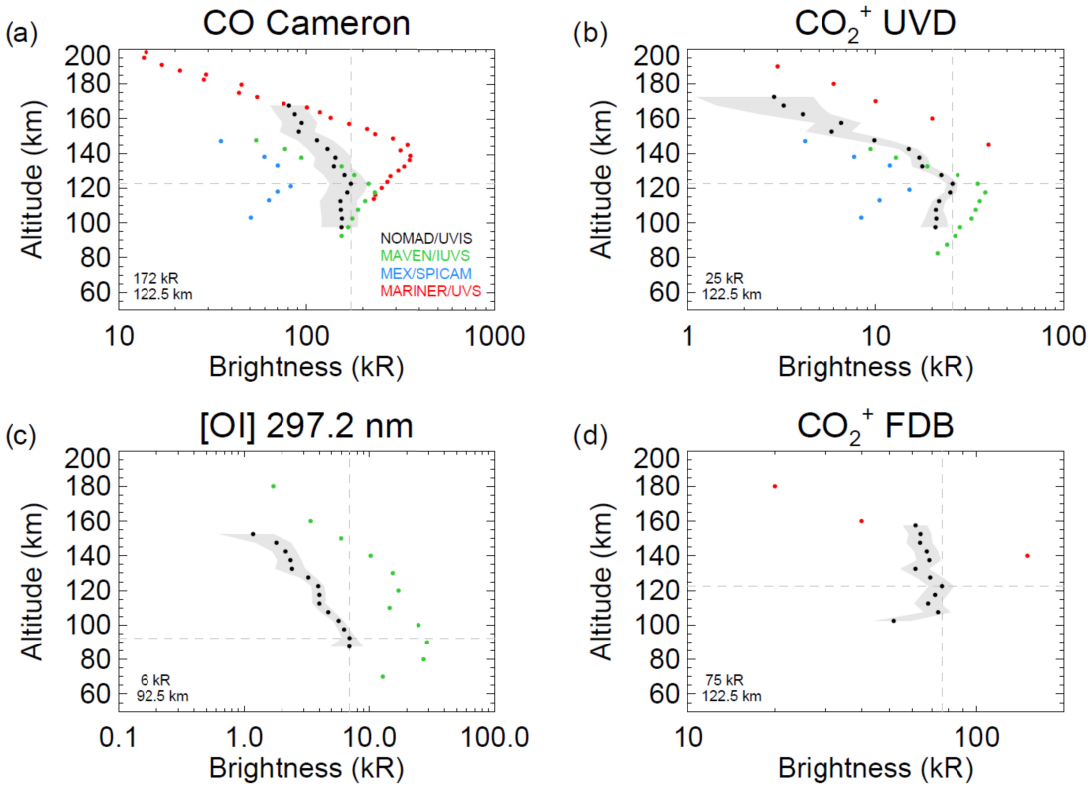

Figure 5: Average limb profiles of the CO Cameron, CO_2^+ UVD, OI 297.2 and CO_2^+ FDB dayglow emissions derived from NOMAD/UVIS observations (black dots). Emission peaks are indicated with dashed lines and brightness and altitude peak values are mentioned on the bottom left part of each panel. Results from earlier missions (MAVEN/IUVS in green, MEx/SPICAM in blue and Mariner/UVS in red) are also indicated for comparison.

5.2. UV emission ratios

Several UV emissions can be observed with the same instrument in the Mars dayglow. Brightness ratios can thus be directly calculated. Using the generated mean limb profiles of Figure 5, it is now possible to deduce intensity ratios of the dayglow emissions. Figure 6 shows these ratios (black dots) as well as some comparisons with results from previous missions (colored dots). It is important to note that while the Cameron and UVD brightness have been extensively measured during the previous decades, it is not the case for the CO_2^+ FDB emission. Thus, the determination of ratios with this emission from simultaneous observations is an important result as described hereafter. Small variations with altitude that can be observed in the plots are not necessarily real: intensities (and thus ratios) are smaller

at low and high altitudes and approach the background noise level. The measured values near the peak of the emissions (between 110 and 130 km) are the most reliable.

As mentioned above, the Cameron/UV doublet ratio has been measured in the past with Mariner, Mex/SPICAM and MAVEN/IUVS (Barth et al 1971; Leblanc et al., 2006; Cox et al., 2010; González-Galindo, 2018; Jain et al., 2015; Gérard et al., 2019). From the UVIS observations, we deduce an average value of 6.6±2.0, consistent with earlier determinations of about 6.7. This value is also in excellent agreement with the mean ratio of 6.6 measured in the nightside discrete aurorae (Soret et al., 2021).

Near the peak of the CO Cameron and CO_2^+ FDB emissions (between 110 and 130 km), a Cameron/FDB ratio of 2.3±0.8 is derived from the UVIS observations (Figure 6b). It agrees relatively well with the nadir model result of 1.5 by Fox and Dalgarno (1979). Finally, this model predicted a value of 2.7 for the CO_2^+ FDB/ CO_2^+ UVD ratio to be compared with our value of 2.8±0.5 and the Mariner ratio of 3.2 (Figure 6c).

In conclusion, UVIS ratios essentially confirm previous measurements and model but are more precise since many more spectra have been included in this study and values are provided versus altitude between 90 and 160 km.

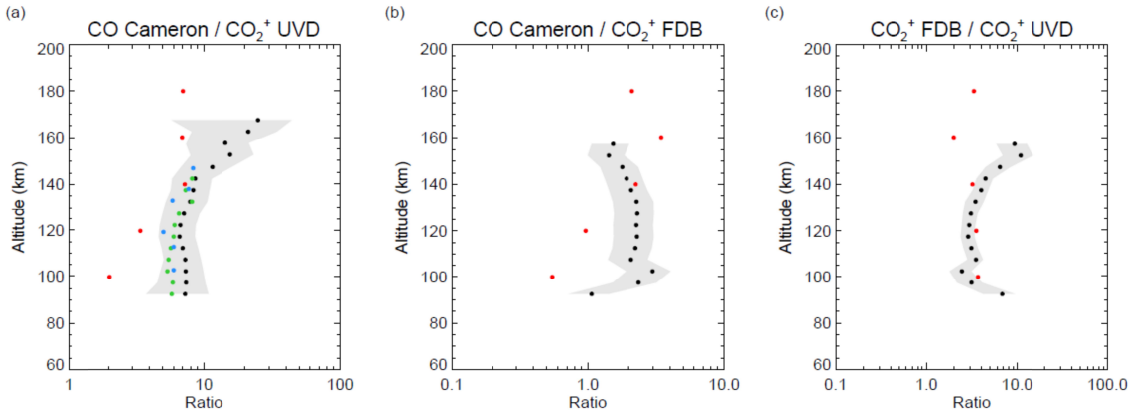

Figure 6: Ratios of the UV emissions derived from NOMAD/UVIS spectra (black dots) and comparison with results from MAVEN/IUVS (green), MEx/SPICAM (blue) and Mariner/UVS (red). The grey color areas represent the absolute uncertainties of the ratios.

5.3. Seasonal variations

In this section, data are now grouped by seasons, in contrast to Section 5.1 where all observations were combined. Figure 7 shows limb profiles of the UV emissions generated according to solar longitude (L_S) and latitude. Thus, the first column corresponds to mean limb profiles in the equatorial region (30° S-30° N), near aphelion (Ls = 71° ± 40 °). The second column shows averaged limb profiles also acquired in the equatorial region, near perihelion (Ls = 251° ± 40°). Finally, column 3 and 4 represent limb profiles derived from summer, respectively in the northern and southern hemispheres (a similar figure can be seen for the visible emissions in Figure 7 of Soret at al., 2022). The rows illustrate, from top to bottom, the CO Cameron (blue), the OI 297.2 (red), the CO_2^+ UVD (green) and the CO_2^+ FDB (purple) emissions. As mentioned by Soret et al. (2022) for the visible dayglow emissions, the UV emissions also exhibit an increase of their peak altitude during the second part of the Martian year (second and fourth columns). This is a consequence of the inflation of the atmosphere when approaching perihelion. We note that the OI emission at 297.2 nm that originates from the same upper state level as the 557.7 nm line described in Soret et al. (2022) also shows two peaks: one near 80-100 km (depending on season) and the other near 100-130 km. Finally, the peak brightness is, as expected, stronger near perihelion (second and fourth columns) than aphelion (first and third columns), due to the increased solar EUV flux reaching the planet during these periods. Only the CO_2^+ FDB limb profiles during the first part of the Martian year (Figures 7m and 7o) are not well defined. The intensity is quite low during this period and spreads over ~100 nm making it more difficult to detect above the background noise level. Only reliable brightness are shown in those plots, which prevents from showing a clear peak in the limb profiles.

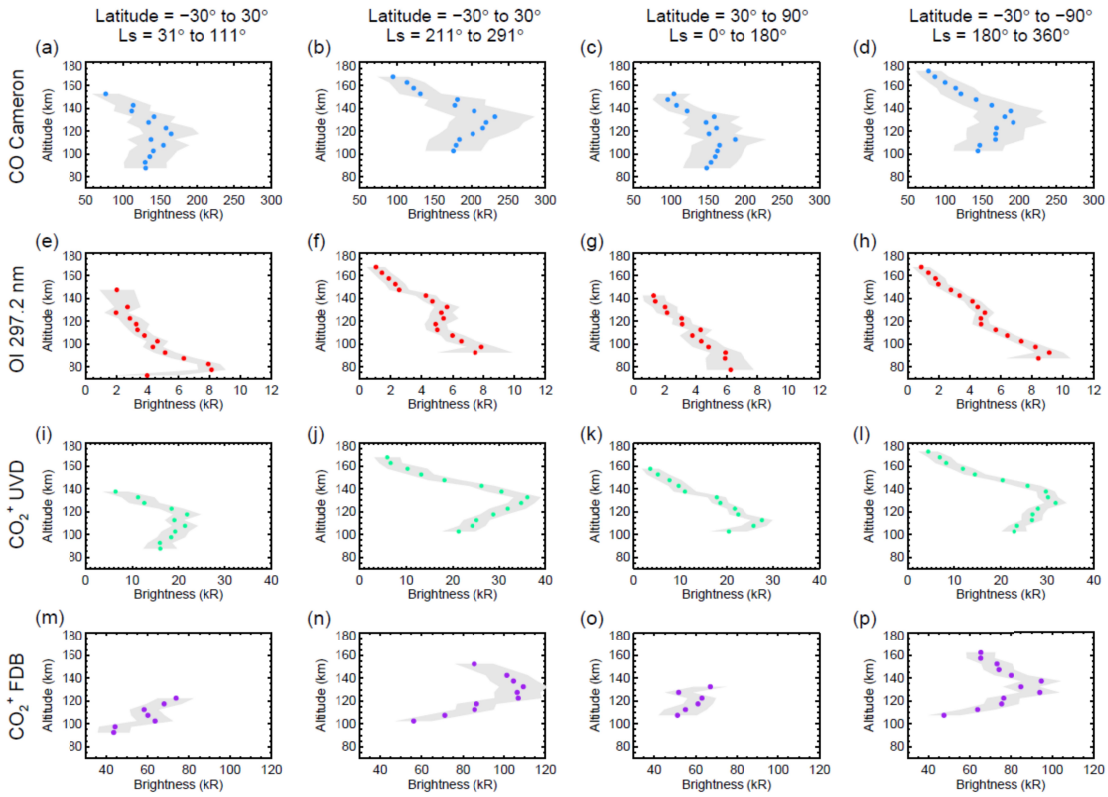

Figure 7: Limb profiles of UV dayglow emissions (Cameron bands in blue, OI 297.2 nm in red, UVD in green and FDB in purple, organized by rows, from top to bottom) averaged in the equatorial region near aphelion (first column) and near perihelion (second column), in the northern summer hemisphere (third column) and during the southern summer (last column).

Another way to illustrate the seasonal variations is to plot the peak parameters (altitude and brightness) of the average limb profiles along solar longitude. All spectra corresponding to a given solar longitude bin are averaged according to their altitude. Emission brightness are then determined from these mean spectra to generate average limb profiles of the UV emissions. The peak altitude and brightness are finally extracted from each average limb profile to study the seasonal variations of these peak parameters. Such plots are presented in Figure 8. The top panels represent the variations of the peak altitude while the bottom ones show the changes of the peak brightness of the UV emissions. The grey lines represent the solar flux with a $1/r^2$ function that has been normalized and shifted to the mean of the observed data points, where r is the Sun-Mars distance. These panels globally demonstrate an increase of both the altitude and the brightness of the emissions near perihelion

(maximum of the grey line). The increase of the peak altitude near perihelion is a consequence of the thermospheric temperature increase and the expansion of the upper atmosphere near perihelion causing the isobar levels to move up (Gérard et al., 2019; Gkouvelis et al., 2020; Soret et al., 2022). The change in altitude is thus expected at this time of the Martian year. The increase in the brightness near perihelion is directly explained by the larger EUV solar photons flux reaching the Martian atmosphere and thus causing enhanced dissociation and ionization during this period. Some variability in the data can be observed and can easily be explained since the observations included in each dot do not share the same properties (latitudes, longitudes, local times and solar zenith angles).

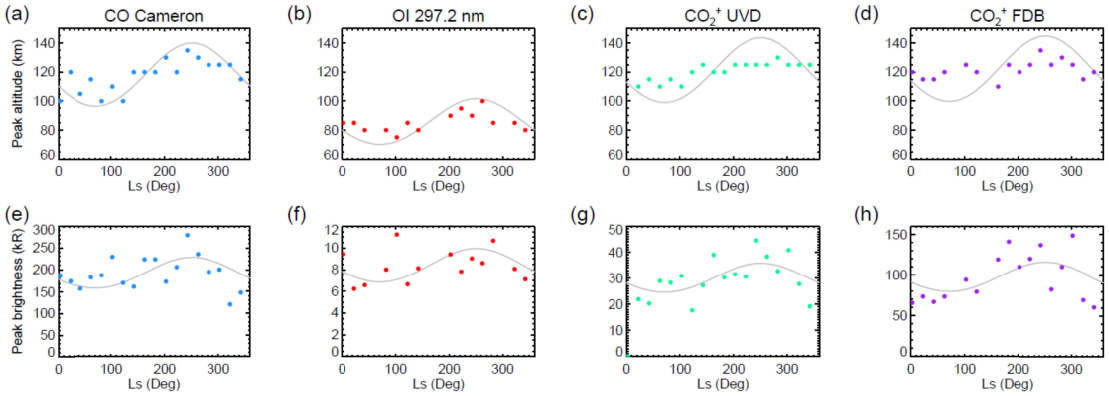

Figure 8: Peak altitudes (top row) and peak brightness (bottom row) of the UV dayglow emissions (Cameron bands in blue, OI 297.2 nm in red, UVD in green and FDB bands in purple) as a function of solar longitude (L_S). The grey lines illustrate the inverse of the square of the Sun-Mars distance, normalized and shifted to the mean of the observed data points. It shows that both quantities generally increase when approaching perihelion (L_S=251°).

6. Sources of the FDB A-X bands

Fox and Dalgarno (1979) explained that the CO_2^+ FDB bands are produced by three mechanisms: photoionization of CO_2, fluorescent scattering of sunlight by CO_2^+ and electron impact ionization of CO_2. Their model estimates that photoionization of CO_2 is the major source of the FDB bands (~60%), while fluorescent scattering produces ~25% of the emission. They conclude that electron impact excitation is a minor source (~15%). Hereafter, we thus decide to neglect this last source, since it remains somewhat marginal, and we do

not expect to be able to finely assess its importance based on the analysis of the recorded spectra. The contributions that we will estimate for the two other mechanisms can then be considered upper bounds, though quite close to the actual values.

The spectral composition of the FDB bands observed in the Mars dayglow during the Mariner 6 and 7 missions have been analyzed by Barth et al. (1971). They compared the spectral distributions expected from solar resonance scattering (fluorescence) and produced in the laboratory by photoionization (Figure 9a). They commented that the observed spectral composition demonstrates that the production of this emission is mainly due to photoionization excitation of CO_2. CO_2^+ fluorescence was estimated to account for only 10% of the total emission. This conclusion was confirmed by model calculations by Stewart et al. (1972).

Cometary spectra showing CO_2^+ bands have later been analyzed by Festou et al. (1982) and Kim (1999) who found that both UVD and FDB systems are excited by fluorescence scattering of CO_2^+ ions. Kim (1999) compared a spectral model of the A-X and B-X bands with observations of comets Austin (1989c1) and P/Giacobini-Zinner. They derived the values of the fluorescence efficiencies (101 g-factors, number of photons scattered per atom in s^{-1}) that can be used to construct a synthetic spectrum based on the relative intensity of the emission bands. Figure 9b shows this spectrum smoothed to the spectral resolution of the UVIS instrument. Comparison with Figure 9a showing the photoionization spectral distribution indicates some important differences. Photoionization mainly populates the FDB bands at shorter wavelengths ((3,0), (2,0) and (1,0) bands) in contrast with fluorescence that populates wavelengths longer than 335 nm (the (1,0), (0,0), (0,1) and (0,2) bands). Here, every 5 km of altitude bin, we minimize the least mean squares of the linear combination of the photoionization and fluorescence spectra to find the best fit of the observed UVIS dayglow spectrum. Our statistical analysis of the best fits indicates that photoionization is the main process producing the FDB bands in the Mars dayglow and contributes ~70 % of the total intensity with a 30% contribution from resonance scattering. This result is in good agreement with Fox and Dalgarno (1979)'s model that estimates photoionization to represent ~60 % of the total CO_2^+ FDB brightness at the peak but not with Barth's analysis of the Mariner spectra. Based only on the (3,0) and (2,0) FDB bands observed with MAVEN/IUVS, Jain et al. (2015) found that the scale heights of the CO_2^+ FDB and UVD

emissions are similar, indicating the same production source. This is consistent with the fact that photoionization produces the UVD emission and largely dominates the shorter wavelengths of the FDB system. However, it does not reflect the fluorescence component observed in the FDB spectral composition at longer wavelengths. Similarly to Stewart et al. (1972)'s analysis, no evidence of a change with altitude in the CO_2^+ FDB spectral composition is observed in the analyzed NOMAD/UVIS spectra.

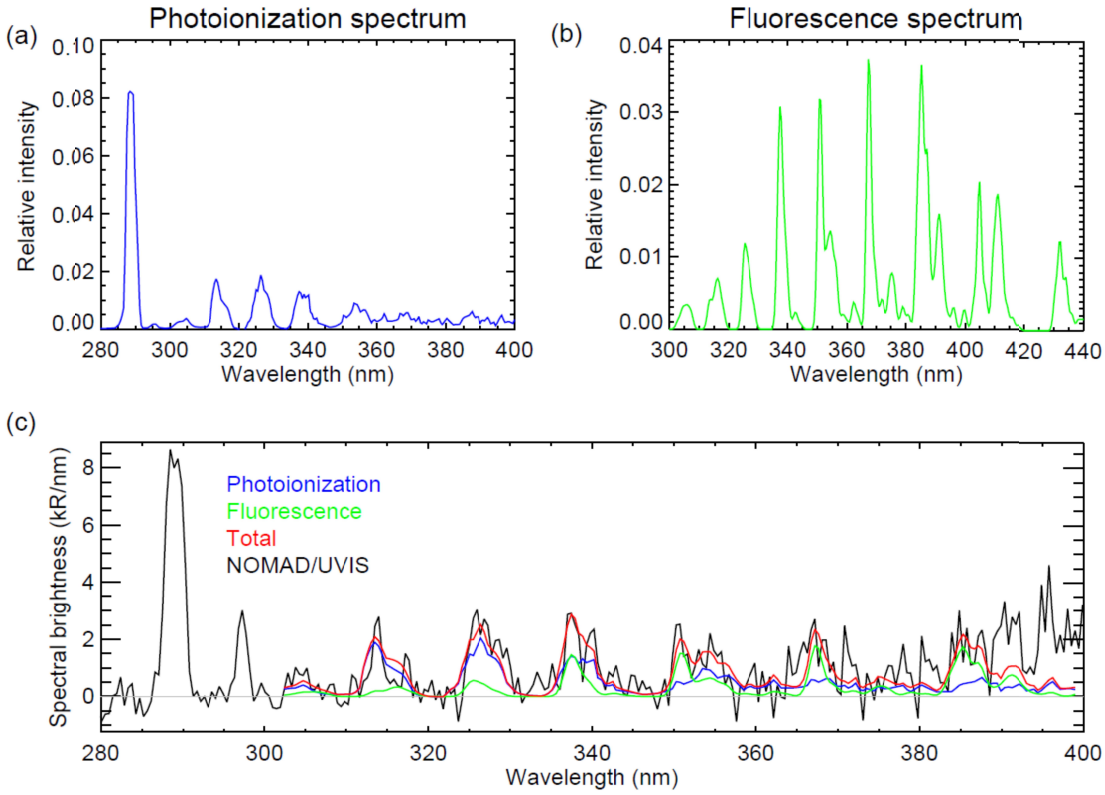

Figure 9: a) Laboratory photoionization spectrum from Barth et al. (1971) for a monochromatic illumination at 58.4 nm, b) Synthetic fluorescence spectrum smoothed to the UVIS spectral resolution (adapted from Kim, 1999), c) Best least mean squares fit of the linear combination of the photoionization (blue, 70%) and fluorescence (green, 30%) spectra (total in red) to match the observed UVIS dayglow spectrum (black) acquired between 125 and 130 km.

7. Conclusions

This study focuses on the UV emissions of the Mars dayglow observed with NOMAD/UVIS. Between 200 and 400 nm, four emissions have been observed: CO Cameron, CO_2^+ UVD and [OI] UV and CO_2^+ FDB. The first three emissions have already been studied with past and ongoing missions, such as Mariner, Mars Express and MAVEN. However, it is the first time that they are simultaneously observed with visible emissions, such as the oxygen green and red line. The oxygen 557.7nm/297.2nm intensity ratio of 15.8 $\pm$ 2.4 has been derived from a large statistical database. The value of this ratio has been controversial, yet it is critical to the calibration of UV and visible instruments. The CO_2^+ FDB emission, however, had not entirely been observed since the Mariner era in the 1970s. A comparison of the NOMAD/UVIS CO_2^+ FDB spectrum with photoionization and resonance scattering spectra confirms that photoionization is the main mechanism for the FDB bands excitation (~70 %). Photoionization populates wavelengths between 300 and 345 nm, but fluorescence makes a non-negligible contribution to the excitation of the longer wavelengths. Our statistical study of this emission has shown that its peak is located between 120 and 140 km, depending on season. We also demonstrate that all the UV dayglow emissions are brighter and occur at higher altitudes when approaching perihelion.

Additionally to the seasonal effect, we expect global dust storm to have a non-negligible impact on the emission characteristics. An increase of the peak brightness and altitude is also expected with a stronger solar activity. Keeping track of these dayglow emissions in the future would thus allow to quantify the interannual variability of these emissions, especially during special events such as dust storms or a stronger solar activity. The dynamics of the upper atmosphere could thus be tracked over time and provide strong constraints to models. Additionally, the main asset of these measurements is to probe the atmosphere at all local times, while other NOMAD instrument measurements mostly occur at the terminator, during solar occultations.

Acknowledgements

The NOMAD experiment is led by the Royal Belgian Institute for Space Aeronomy (IASB-BIRA), assisted by Co-PI teams from Spain (IAA-CSIC), Italy (INAF-IAPS), and the United Kingdom (Open

University). This project acknowledges funding by the Belgian Science Policy Office (BELSPO), with the financial and contractual coordination by the ESA Prodex Office (PEA 4000103401, 4000121493, 4000129686), as well as by UK Space Agency funding through grants ST/V002295/1, ST/V005332/1 and ST/S00145X/1. This research was supported by the Belgian Fonds de la Recherche Scientifique – FNRS under Grant No. 30442502 (ET_HOME). B. H. is supported by the Belgian Fund for Scientific Research (FNRS). The MAVEN mission is supported by NASA in association with the University of Colorado and NASA's Goddard Space Flight Center.

Open Research

Data - The IUVS data may be downloaded from the Planetary Atmospheres Node of the Planetary Data System (PDS, Deighan; 2018). The NOMAD SO, LNO and UVIS datasets are available on the ESA Planetary Science Archive at https://archives.esac.esa.int/psa/#!Table%20View/NOMAD=instrument for all data since the beginning of the nominal science mission (21 April 2018).

Repository - The results retrieved from the NOMAD measurements used in this article are available on the BIRA-IASB data repository (Soret & Vandaele, 2023).

References

Aoki, S., Gkouvelis, L., Gérard, J.-C., Soret, L., Hubert, B., Lopez-Valverde, M. A., et al. (2022). Density and temperature of the upper mesosphere and lower thermosphere of Mars retrieved from the OI 557.7 nm dayglow measured by TGO/NOMAD. Journal of Geophysical, Research: Planets, 127, e2022JE007206. https://doi.org/10.1029/2022JE007206

Barth, C.A., Hord, C.W., Pearce, J.B., Kelly, K.K., Anderson, G.P., Stewart, A.I., Mariner 6 and 7 ultraviolet spectrometer experiment: Upper atmosphere data, J. Geophys. Res., 76 (1971), p. 2213

Barth, C.A., Hord, C.W., Stewart, A.I., Lane, A.L., Mariner 9 ultraviolet spectrometer experiment: Initial results, Science, 175 (1972), pp. 309-312

Bertaux, J.L. et al., SPICAM on Mars Express: Observing modes and overview of UV spectrometer data and scientific results, J. Geophys. Res., 111 (2006), p. 10

Cox, C., Gérard, J.-C., Hubert, B., Bertaux, J.-L., Bougher, S.W., Mars ultraviolet dayglow variability: SPICAM observations and comparison with airglow model, J. Geophys. Res., 115 (2010), p. 4010

Deighan, J. (2018). Mars Atmosphere and Volatile Evolution (MAVEN) Imaging Ultraviolet Spectrograph (IUVS) Processed-level Data Product Bundle [Data]. NASA Planetary Data System. https://doi.org/10.17189/1518964

Feldman, P.D., Burgh, E.B., Durrance, S.T., Davidsen, A.F., Far ultraviolet spectroscopy of Venus and Mars at 4 Å resolution with the Hopkins ultraviolet telescope on Astro-2, Astrophys. J., 538 (2000), pp. 95-400

Festou, M. C., Feldman, P. D., & Weaver, H. A. (1982). The ultraviolet bands of the CO_2^+ ion in comets. The Astrophysical Journal, 256, 331-338.

Fox, J. L. and Dalgarno, A. (1979), Ionization, Luminosity, and Heating of the Upper Atmosphere of Mars, 84, A12, Journal of Geophysical Research

607 Gattinger, R. L. et al. (2009), Observation of the 557.7 nm to 297.2 nm brightness ratio in the
608 auroral spectrum with OSIRIS on Odin. Can. J. Phys. 87, 1133–1137.
609
610 Gérard, J. C., Gkouvelis, L., Ritter, B., Hubert, B., Jain, S. K., & Schneider, N. M. (2019). MAVEN-
611 IUVS observations of the CO2 + UV doublet and CO Cameron bands in the Martian thermosphere:
612 Aeronomy, seasonal, and latitudinal distribution. Journal of Geophysical Research: Space Physics,
613 124(7), 5816–5827.
614
615 Gérard, J. C., Aoki, S., Willame, Y., Gkouvelis, L., Depiesse, C., Thomas, I. R., et al. (2020).
616 Detection of green line emission in the dayside atmosphere of Mars from NOMAD-TGO observations.
617 Nature Astronomy, 4(11), 1049–1052.
618
619 Gérard, J. C., Aoki, S., Gkouvelis, L., Soret, L., Willame, Y., Thomas, I. R., et al. (2021). First
620 observation of the oxygen 630 nm emission in the Martian dayglow. Geophysical Research Letters,
621 48(8), e2020GL092334. https://doi.org/10.1029/2020GL092334
622
623 Gkouvelis, L., Gérard, J. C., Ritter, B., Hubert, B., Schneider, N. M., & Jain, S. K. (2018). The O(^{1}S)
624 297.2-nm dayglow emission: A tracer of CO_2 density variations in the martian lower thermosphere.
625 Journal of Geophysical Research: Planets, 123(12), 3119–3132.
626
627 Gkouvelis, L., Gérard, J. C., Ritter, B., Hubert, B., Schneider, N. M., & Jain, S. K. (2020). Airglow
628 remote sensing of the seasonal variation of the martian upper atmosphere: MAVEN limb
629 observations and model comparison. Icarus, 341, 113666.
630
631 González-Galindo, F., Chaufray, J.-Y.,Forget, F., García-Comas, M.,Montmessin, F., Jain, S. K., &
632 Stiepen, A. (2018). UV dayglow variability onMars: Simulation with a global climate model and
633 comparison with SPICAM/MEx data, Journal of Geophysical Research: Planets,123, 1934–1952.
634 https://doi.org/10.1029/2018JE005556
635
636 Jain, S.K. and Bhardwaj, A., Impact of solar EUV flux on CO Cameron band and CO_2^+ UV doublet
637 emissions in the dayglow of Mars, Planet. Space Sci., 63–64 (2012), pp. 110-122,
638 https://doi.org/10.1016/j.pss.2011.08.010
639

Jain, S. K., et al. (2015), The structure and variability of Mars upper atmosphere as seen in MAVEN/IUVS dayglow observations, Geophys. Res. Lett., 42, 9023–9030, doi:10.1002/2015GL065419

Kim, S. J. (1999). Fluorescence efficiencies of the AX and BX systems of CO_2^+ in comets. Earth, planets and space, vol. 51, no 2, p. 139-145.

Kramida, A. (2022). Atomic Transition Probability Bibliographic Database (version 9.0), https://physics.nist.gov/Elevbib. National Institute of Standards and Technology, Gaithersburg, MD; DOI: 10.18434/T46C7N

Leblanc, F., Chaufray, J.Y., Lilensten, J., Witasse, O., Bertaux, J.-L., Martian dayglow as seen by the SPICAM UV spectrograph on Mars Express, J. Geophys. Res., 111 (2006), p. 9

McClintock, W. E., Schneider, N. M., Holsclaw, G. M., Clarke, J. T., Hoskins, A. C., Stewart, I., et al. (2015). The Imaging Ultraviolet Spectrograph (IUVS) for the MAVEN mission. Space Science Reviews, 195(1–4), 75–124. https://doi.org/10.1007/s11214-014-0098-7

Millour, E., Spiga, A., Colaitis, A., Navarro, T., Madeleine, J.-B., Chaufray, J.-Y., et al., (2012). Mars Climate Database Version 5, in: European Planetary Science Congress 2012. p. 302.

Montmessin, F., Korablev, O., Lefèvre, F., Bertaux, J. L., Fedorova, A., Trokhimovskiy, A., Chaufray, J.-Y., Lacombe, G., Reberac, A., Maltagliati, L., Willame, Y., Guslyakova, S., Gérard, J.-C., Stiepen, A., Fussen, D., Mateshvili, N., Määttänen, A., Forget, F., Witasse, O., Leblanc, F. Vandaele, A. C., Marcq, E., Sandel, B., Gondet, B., Schneider, N., Chaffin, M. and Chapron, N. (2017). SPICAM on Mars Express: A 10 year in-depth survey of the Martian atmosphere. Icarus, 297, 195-216.

Patel, M. R., Antoine, P., Mason, J., Leese, M., Hathi, B., Stevens, A. H., et al. (2017). NOMAD spectrometer on the ExoMars trace gas orbiter mission: Part 2—Design, manufacturing, and testing of the ultraviolet and visible channel. Applied Optics, 56(10), 2771–2782, https://doi.org/10.1364/AO.56.002771

Schneider, N., Milby, Z., Jain, S. K., González-Galindo, F., Royer, E., Gérard, J. C., et al. (2020). Imaging of Martian circulation patterns and atmospheric tides through MAVEN/IUVS nightglow

observations. Journal of Geophysical Research: Space Physics, 125, e2019JA027318. https://doi.org/10.1029/2019JA027318

Schneider, N. M., Milby, Z., Jain, S. K., Gérard, J.-C., Soret, L., Brain, D. A., et al. (2021). Discrete aurora on Mars: Insights into their distribution and activity from MAVEN/IUVS observations. Journal of Geophysical Research: Space Physics, 126, e2021JA029428. https://doi.org/10.1029/2021JA029428

Shematovich, V.I., Bisikalo, D.V., Gérard, J.-C., Cox, C., Bougher, S.W., Leblanc, F., Monte Carlo model of electron transport for the calculation of Mars dayglow emissions, J. Geophys. Res., 113 (2008), pp. 2156-2202, 10.1029/2007JE002938

Simon, C., Witasse, O., Leblanc, F., Gronoff, G., Bertaux, J.-L., Dayglow on Mars: Kinetic modeling with SPICAM UV limb data, Planet. Space Sci., 57 (2009), pp. 1008-1021

Slanger, T. G., Cosby, P. C., Sharpee, B. D., Minschwaner, K. R. and Siskind, D. E. (2006), O(^{1}S→ ^{1}D, ^{3}P) branching ratio as measured in the terrestrial nightglow. J. Geophys. Res. 111, A12318.

Soret, L., Gérard, J.-C., Schneider, N., Jain, S., Milby, Z., Ritter, B., et al. (2021). Discrete aurora on Mars: Spectral properties, vertical profiles, and electron energies. Journal of Geophysical Research: Space Physics, 126, e2021JA029495. https://doi.org/10.1029/2021JA029495

Soret, L., Gérard, J.-C., Aoki, S., Gkouvelis, L., Thomas, I. R., Ristic, B., et al. (2022). The Mars oxygen visible dayglow: A Martian year of NOMAD/UVIS observations. Journal of Geophysical Research: Planets, 127, e2022JE007220. https://doi.org/10.1029/2022JE007220

Soret, L. and Vandaele, A. C. (2023). Dataset of the retrieved UV emissions from TGO/NOMAD/UVIS dayside limb observations, presented in Soret et al., 2023 [Data]. Royal Belgian Institute for Space Aeronomy. https://dx.doi.org/10.18758/71021081

Stewart, A.I., Mariner 6 and 7 ultraviolet spectrometer experiment: Implications of CO_2^+, CO and O airglow, J. Geophys. Res., 77 (1972), p. 54

706 Stewart, A. I., Barth, C. A., Hord, C. W., & Lane, A. L. (1972). Mariner 9 ultraviolet spectrometer
707 experiment: Structure of Mars' upper atmosphere. Icarus, 17(2), 469-474.
708
709 Stiepen, A., Gérard, J.-C., Bougher, S., Montmessin, F., Hubert, B., & Bertaux, J.-L. (2015). Mars
710 thermospheric scale height: CO Cameron and CO_2^+ dayglow observations from Mars Express. Icarus,
711 245, 295–305. https://doi.org/10.1016/j.icarus.2014.09.051
712
713 Swings, P., & Page, T. (1950). The Spectrum of Comet Bester (1947k). Astrophysical Journal, 111 ,
714 530-554.
715
716 Vandaele, A. C., López -Moreno, J.-J., Patel, M. R., Bellucci, G., Daerden, F., Ristic, B., et al.
717 (2018a). NOMAD, an integrated suite of spectrometers for the ExoMars Trace Gas Mission: Technical
718 description, science objectives, and expected performance. Space Science Reviews, 214(5),
719 https://doi.org/10.1007/s11214-018-0517-2
720
721 Vandaele, A. C., Neefs, E., Drummond, R., Thomas, I. R., Daerden, F., López-Moreno, J. J., et al.
722 (2018b). Science objectives and performances of NOMAD, a spectrometer suite for the ExoMars TGO
723 mission. Planetary and Space Science, 119, 233–249. https://doi.org/10.1016/j.pss.2015.10.003
724
725 Willame, Y., Depiesse, C., Mason, J. P., Thomas, I. R., Patel, M. R., Hathi, B., Leese, M. R., Bolsée,
726 D., Wolff, M. J., Trompet, L., Vandaele, A. C., Piccialli, A., Aoki, S., Ristic, B., Neefs, E., Beeckman, B.,
727 Berkenbosch, S., Clairquin, R., Mahieux, A., Pereira, N., Robert, S., Viscardy, S., Wilquet, V., Daerden,
728 F., Lopez-Moreno, J. J., Bellucci, G. (2022). Calibration of the NOMAD-UVIS data, Planetary and Space
729 Science, Volume 218, 105504, https://doi.org/10.1016/j.pss.2022.105504.

Figure 1.

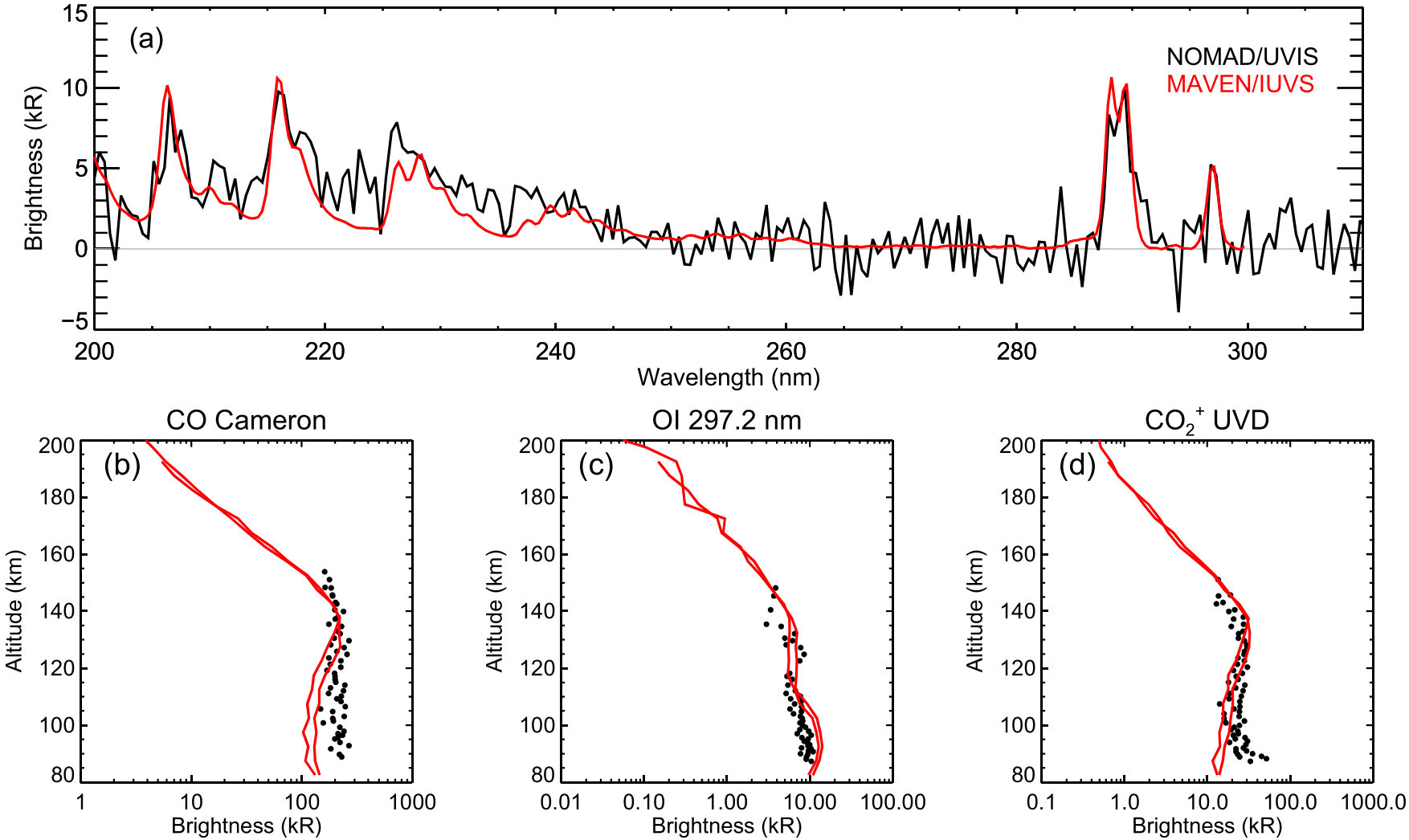
(a)
NOMAD/UVIS
MAVEN/IUVS
Brightness (kR)
Wavelength (nm)
CO Cameron
(b)
OI 297.2 nm
(c)
CO_2^+ UVD
(d)
Altitude (km)
Brightness (kR)

Figure 2.

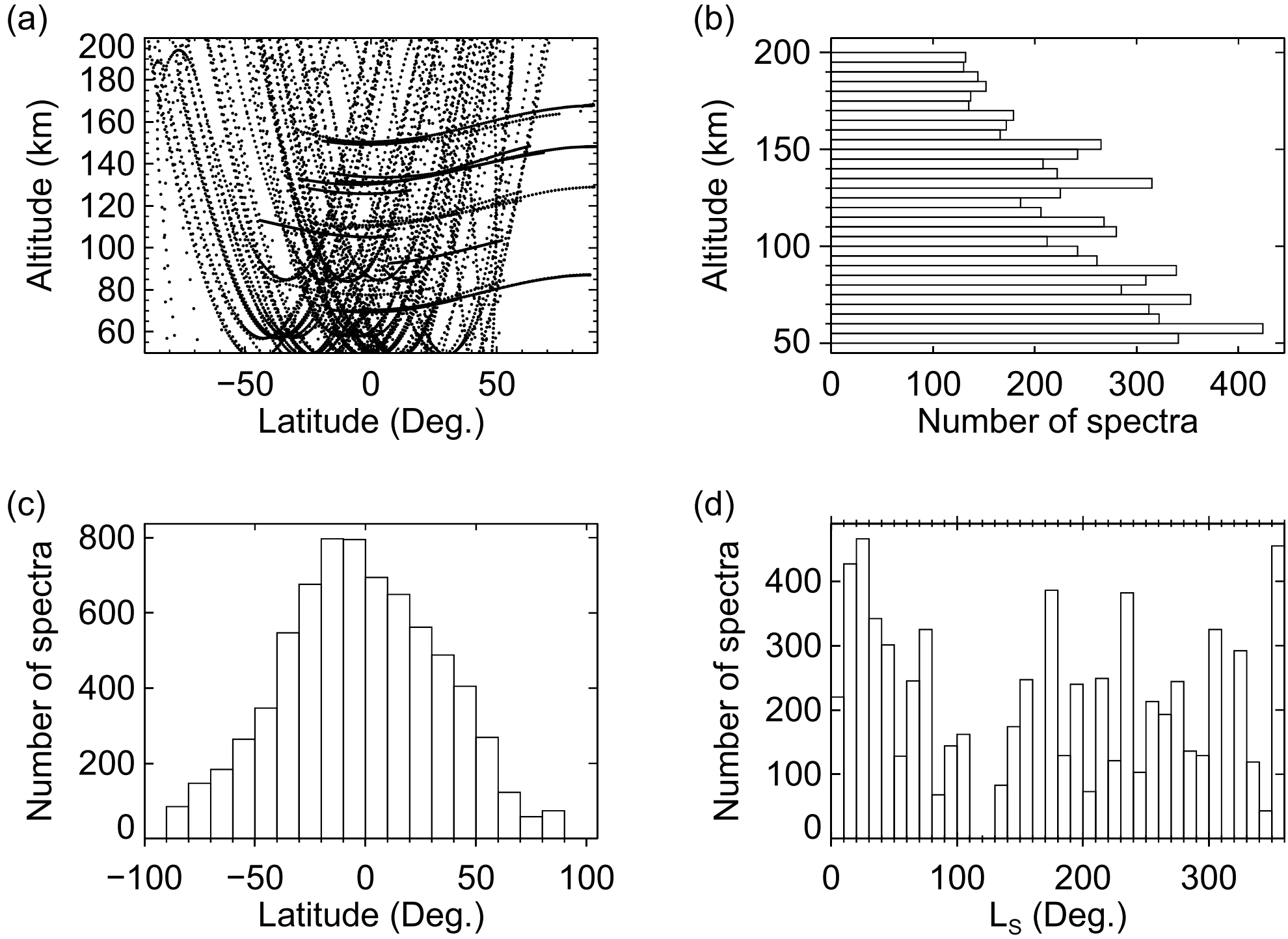
(a)
Altitude (km)
200
180
160
140
120
100
80
60
−50
0
50
Latitude (Deg.)
(b)
Altitude (km)
200
150
100
50
0
100
200
300
400
Number of spectra
(c)
Number of spectra
800
600
400
200
0
−100
−50
0
50
100
Latitude (Deg.)
(d)
Number of spectra
400
300
200
100
0
0
100
200
300
L_S (Deg.)

Figure 3.

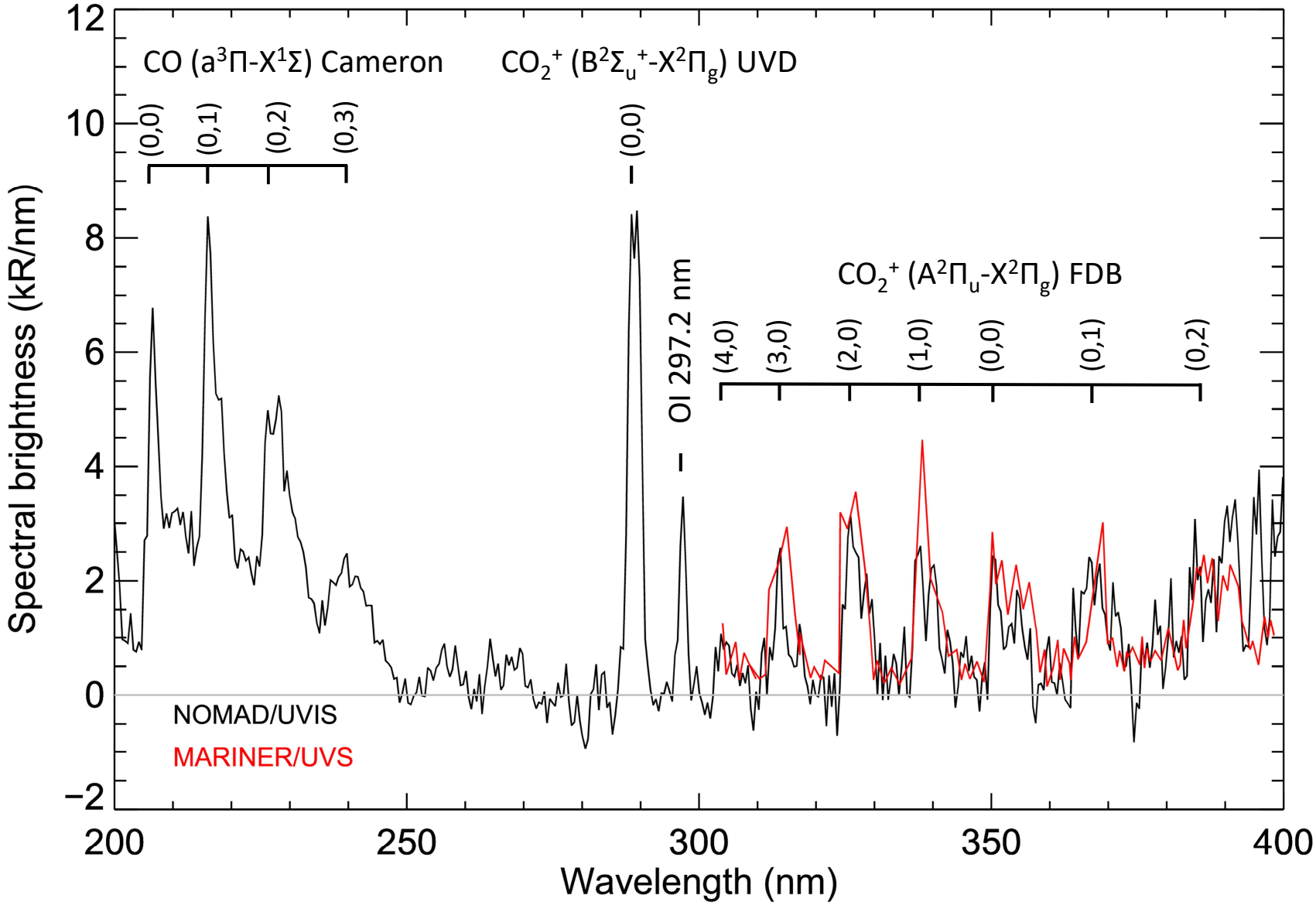
CO (a³Π-X¹Σ) Cameron
CO2+ (B2Σu+-X2Πg) UVD
(0,0)
(0,1)
(0,2)
(0,3)
(0,0)
OI 297.2 nm
CO2+ (A2Πu-X2Πg) FDB
(4,0)
(3,0)
(2,0)
(1,0)
(0,0)
(0,1)
(0,2)
NOMAD/UVIS
MARINER/UVS
Spectral brightness (kR/nm)
Wavelength (nm)
12
10
8
6
4
2
0
−2
200
250
300
350
400

Figure 4.

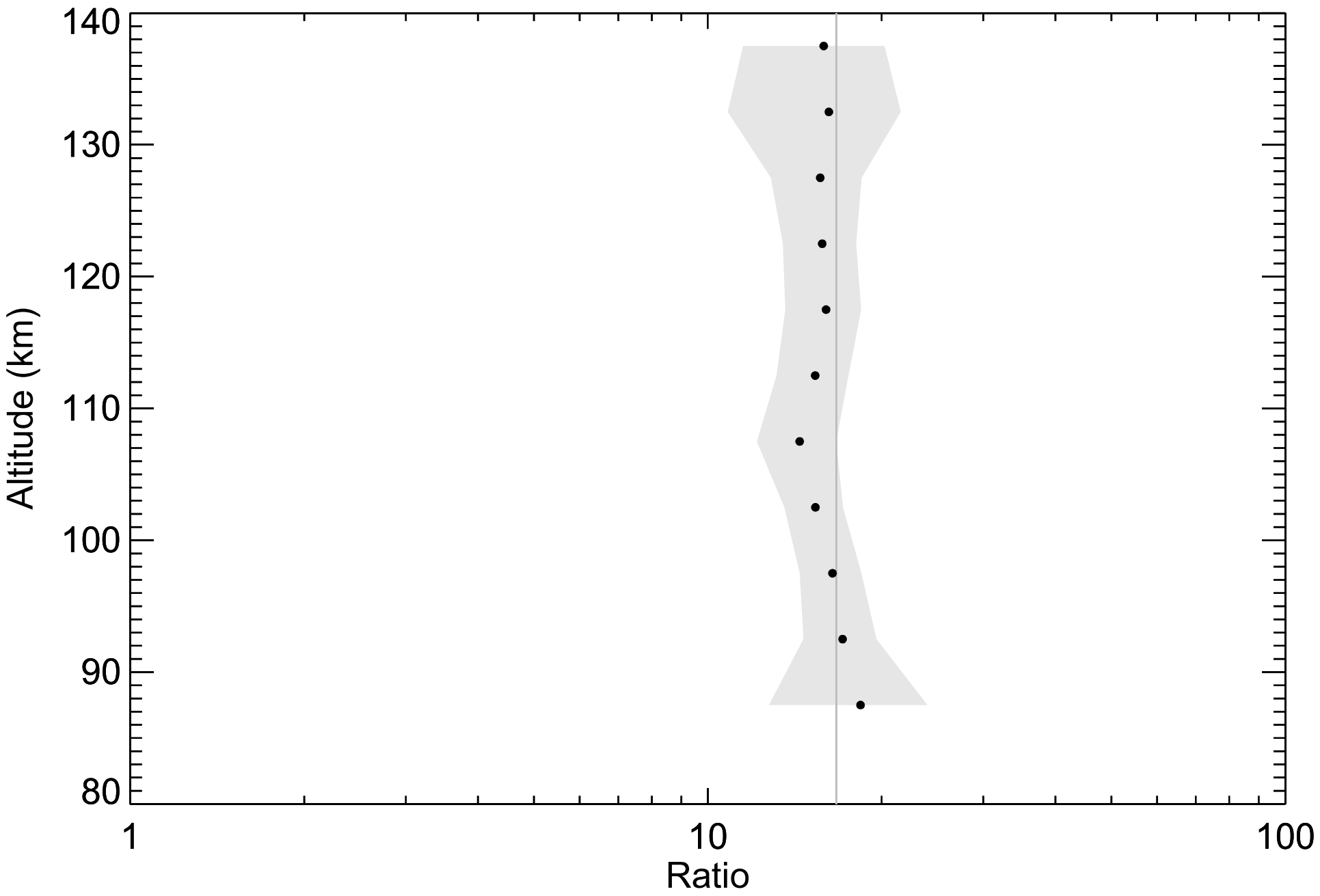
140
130
120
110
100
90
80
Altitude (km)
1
10
100
Ratio

Figure 5.

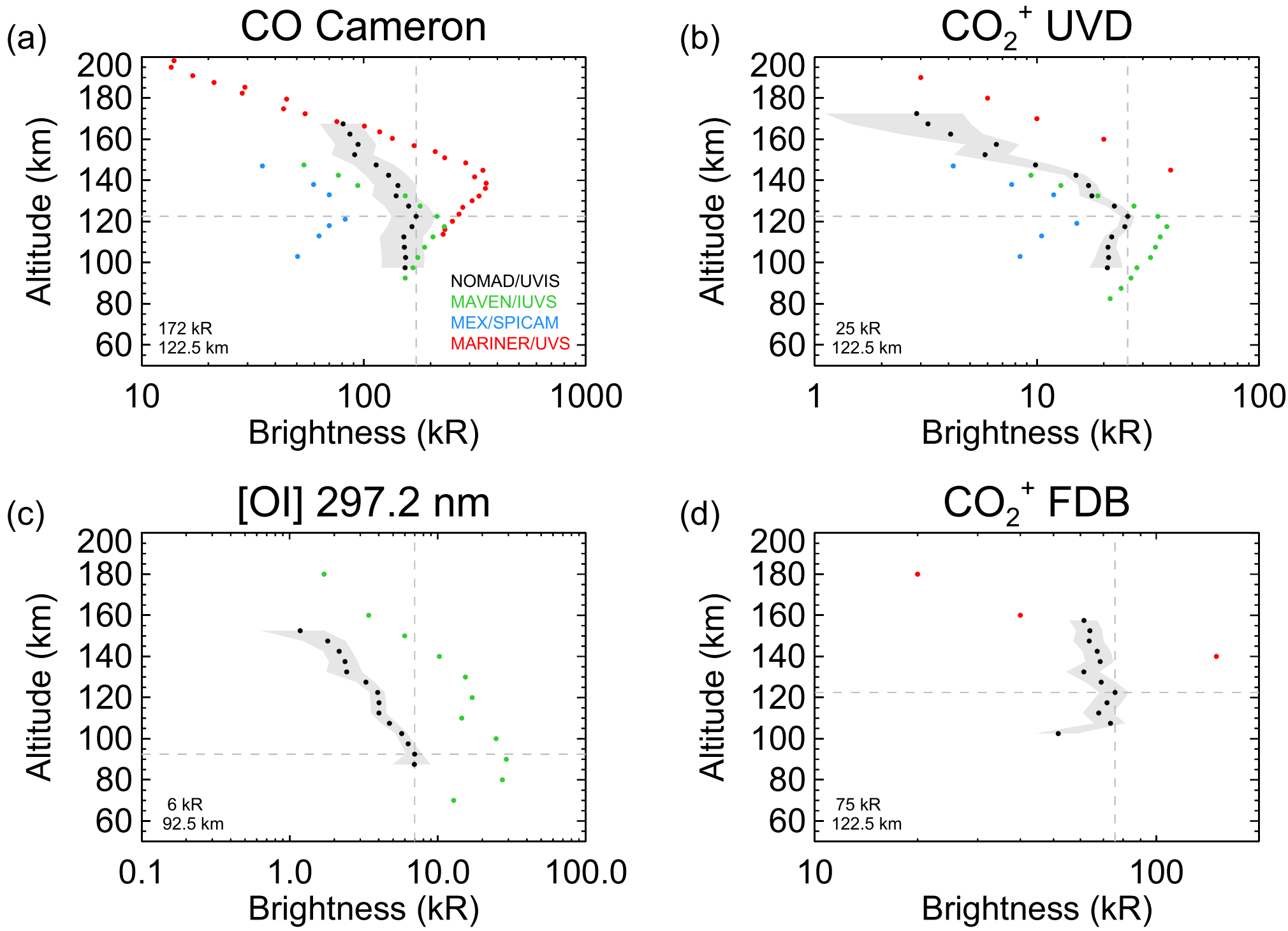
(a)
CO Cameron
Altitude (km)
200
180
160
140
120
100
80
60
10
100
1000
Brightness (kR)
172 kR
122.5 km
NOMAD/UVIS
MAVEN/IUVS
MEX/SPICAM
MARINER/UVS
(b)
CO_2^+ UVD
Altitude (km)
1
10
100
Brightness (kR)
25 kR
122.5 km
(c)
[OI] 297.2 nm
Altitude (km)
0.1
1.0
10.0
100.0
Brightness (kR)
6 kR
92.5 km
(d)
CO_2^+ FDB
Altitude (km)
10
100
Brightness (kR)
75 kR
122.5 km

Figure 6.

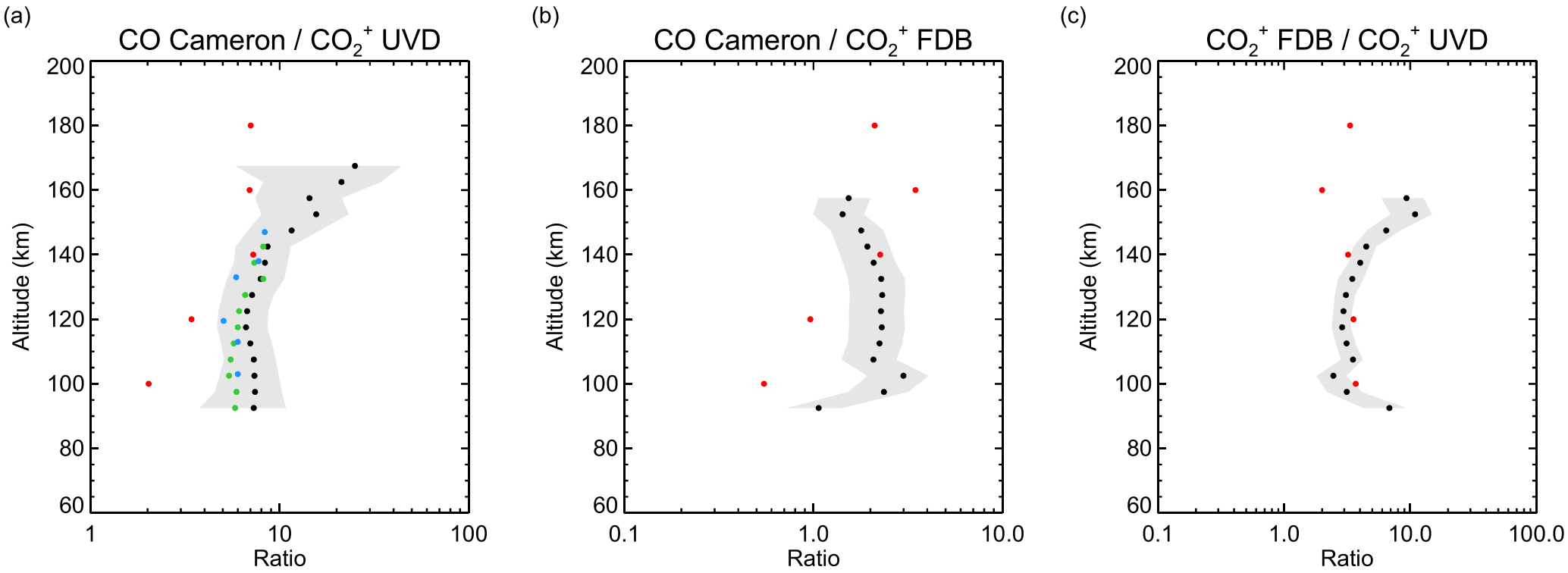
(a)
CO Cameron / CO_2^+ UVD
Altitude (km)
200
180
160
140
120
100
80
60
1
10
100
Ratio
(b)
CO Cameron / CO_2^+ FDB
Altitude (km)
200
180
160
140
120
100
80
60
0.1
1.0
10.0
Ratio
(c)
CO_2^+ FDB / CO_2^+ UVD
Altitude (km)
200
180
160
140
120
100
80
60
0.1
1.0
10.0
100.0
Ratio

Figure 7.

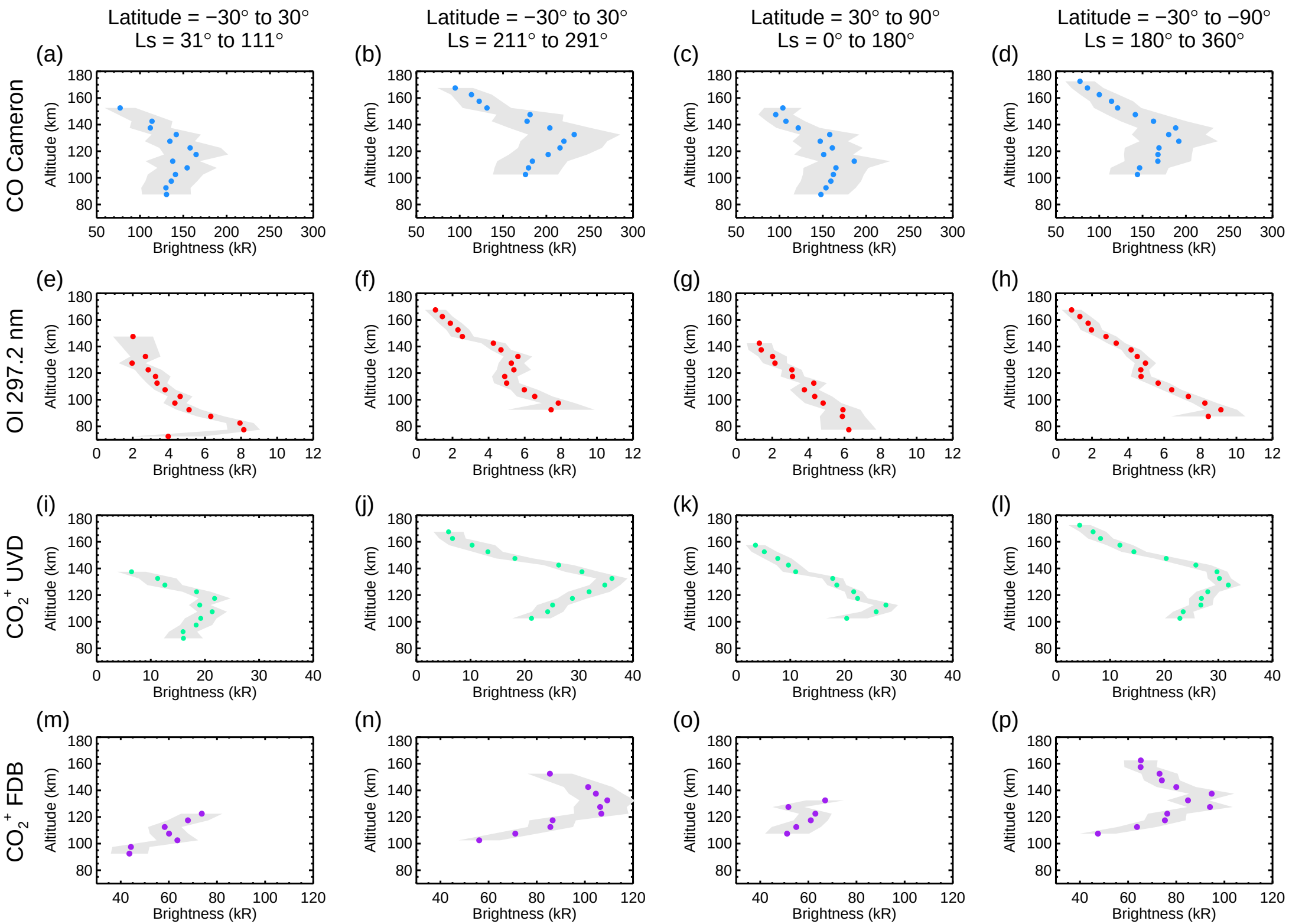
Latitude = −30° to 30°
Ls = 31° to 111°
Latitude = −30° to 30°
Ls = 211° to 291°
Latitude = 30° to 90°
Ls = 0° to 180°
Latitude = −30° to −90°
Ls = 180° to 360°
(a)
(b)
(c)
(d)
(e)
(f)
(g)
(h)
(i)
(j)
(k)
(l)
(m)
(n)
(o)
(p)
CO Cameron
OI 297.2 nm
CO_2^+ UVD
CO_2^+ FDB
Altitude (km)
Brightness (kR)

Figure 8.

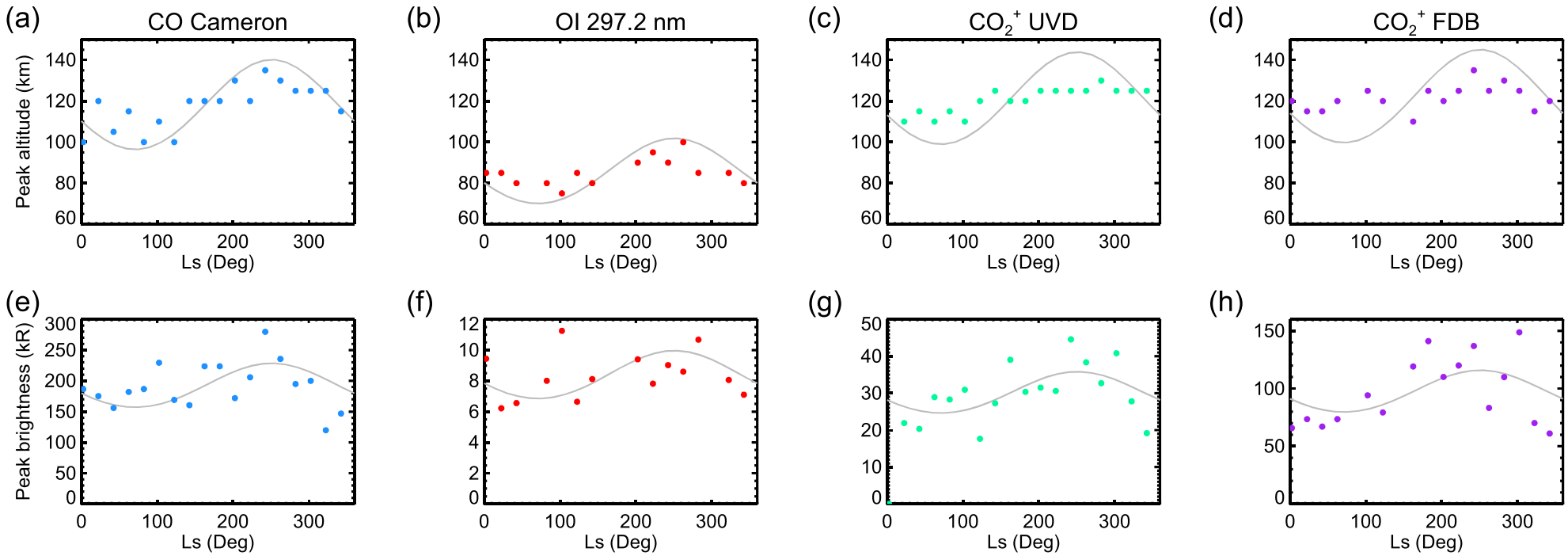
(a)
CO Cameron
(b)
OI 297.2 nm
(c)
CO_2^+ UVD
(d)
CO_2^+ FDB
Peak altitude (km)
(e)
(f)
(g)
(h)
Peak brightness (kR)
Ls (Deg)

Figure 9.

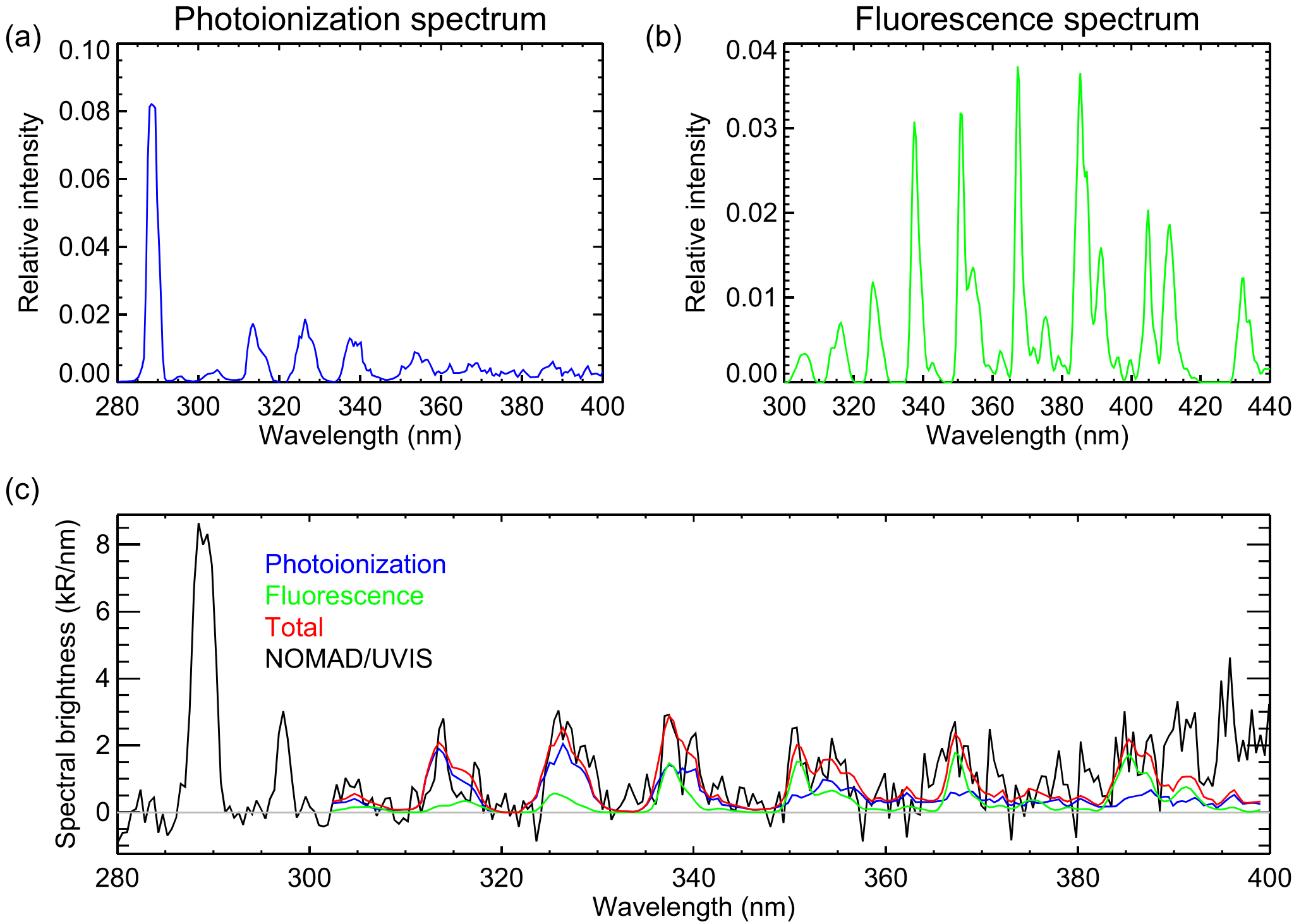
(a)
Photoionization spectrum
Relative intensity
0.10
0.08
0.06
0.04
0.02
0.00
280
300
320
340
360
380
400
Wavelength (nm)
(b)
Fluorescence spectrum
Relative intensity
0.04
0.03
0.02
0.01
0.00
300
320
340
360
380
400
420
440
Wavelength (nm)
(c)
Spectral brightness (kR/nm)
8
6
4
2
0
Photoionization
Fluorescence
Total
NOMAD/UVIS
280
300
320
340
360
380
400
Wavelength (nm)